Nematic twist–bend phase in an external field

Grzegorz Pająk[a,b,1], Lech Longa[a,1], and Agnieszka Chrzanowska[b,1]

[a]Marian Smoluchowski Institute of Physics, Department of Statistical Physics, Jagiellonian University, 30-348 Kraków, Poland; and [b]Faculty of Physics, Mathematics, and Computer Science, Tadeusz Kościuszko Cracow University of Technology, 30-084 Kraków, Poland

Edited by Ivan Dozov, Université Paris-Sud, Orsay, France, and accepted by Editorial Board Member John D. Weeks September 10, 2018 (received for review December 15, 2017)

The response of the nematic twist–bend (N_{TB}) phase to an applied field can provide important insight into the structure of this liquid and may bring us closer to understanding mechanisms generating mirror symmetry breaking in a fluid of achiral molecules. Here we investigate theoretically how an external uniform field can affect structural properties and the stability of N_{TB}. Assuming that the driving force responsible for the formation of this phase is packing entropy, we show, within Landau–de Gennes theory, that N_{TB} can undergo a rich sequence of structural changes with the field. For the systems with positive anisotropy of permittivity, we first observe a decrease of the tilt angle of N_{TB} until it transforms through a field-induced phase transition to the ordinary prolate uniaxial nematic phase (N). Then, at very high fields, this nematic phase develops polarization perpendicular to the field (N_{p+}). For systems with negative anisotropy of permittivity, the results reveal new modulated structures. Even an infinitesimally small field transforms N_{TB} to its elliptical counterpart (N_{TBe}), where the circular base of the cone of the main director becomes elliptic. With stronger fields, the ellipse degenerates to a line, giving rise to a nonchiral periodic structure, the nematic splay–bend (N_{SB}), where the two nematic directors are restricted to a plane. The three structures—N_{TB}, N_{TBe}, and N_{SB}—with a modulated polar order are globally nonpolar. But further increase of the field induces phase transitions into globally polar structures with nonvanishing polarization along the field's direction. We found two such structures, one of which is a polar and chiral modification of N_{SB}, where splay and bend deformations are accompanied by weak twist deformations ($N^{*}_{SB_p}$). Further increase of the field unwinds this structure into a polar nematic (N_{p-}) of polarization parallel to the field.

nematics | twist–bend | splay–bend | chirality | polarity

The twist–bend nematic (N_{TB}) phase, recently discovered in liquid crystalline chemically achiral dimers (1–7), bent-core mesogens (8, 9), and their hybrids (10), is one of the most amazing examples of spontaneous chiral symmetry breaking in soft-matter physics. It occurs in the liquid state without any long-range positional order, but the average local molecular long axis, $\hat{\mathbf{n}}$, known as the director, follows a nanoscale-pitch heliconical winding. Thus, the structure belongs to the family of nematic phases and is the fifth nematic phase recognized (5), in addition to uniaxial and biaxial nematics for nonchiral liquid crystalline materials and cholesteric and blue phases for chiral liquid crystals (11). In 2001, Dozov (12), following earlier analysis of Meyer (13, 14), predicted theoretically this structure using the Frank model of elastic deformations in nematics by assuming that the bend elastic constant can change sign. With this assumption, $\hat{\mathbf{n}}$ can form 1D modulated structures where simultaneously twist and bend or splay and bend are nonzero. The second of the structures, known as the nematic splay–bend (N_{SB}), is nonchiral and exhibits periodic splay and bend modulations of the director, taking place within one plane. The observation of this phase is still not confirmed experimentally, but it can be stabilized in constant-pressure Monte Carlo simulations of thin layers composed of hard bent–core molecules (15).

The first possibility is recognized as the chiral N_{TB} phase, with the director, $\hat{\mathbf{n}}(\mathbf{r}) \equiv \hat{\mathbf{n}}(z)$, attaining an oblique helicoidal structure in precessing on the side of a right circular cone (Fig. 1). More specifically,

$$\hat{\mathbf{n}}(z) = [\cos(\phi_{\hat{\mathbf{n}}})\sin(\theta_{\hat{\mathbf{n}}}), \sin(\phi_{\hat{\mathbf{n}}})\sin(\theta_{\hat{\mathbf{n}}}), \cos(\theta_{\hat{\mathbf{n}}})], \qquad [1]$$

where $\theta_{\hat{\mathbf{n}}}$ is the conical angle (angle between $\hat{\mathbf{n}}$ and $\mathbf{k}$) and $\phi_{\hat{\mathbf{n}}} = \pm kz = \pm\frac{2\pi}{p}z$, with wave vector $\mathbf{k} = k\hat{\mathbf{z}}$ taken to be parallel to the $\hat{\mathbf{z}}$ axis of the laboratory system of frame; here, p is the pitch. The Dozov's theory (12) of the N_{TB} phase has strong experimental support for anomalously small (but positive) bend elastic constant that has been reported in the vicinity of the nematic-nematic twist-bend phase transition (4, 16). The Landau–de Gennes (LdeG) mesoscopic theory, where the director is replaced by a symmetric and traceless tensor order parameter field, $\tilde{\mathbf{Q}}$, often referred to as the alignment tensor, accounts for a fine structure of the modulated phases and shows limitations of the director's description (17, 18). The eigenvector of $\tilde{\mathbf{Q}}$ corresponding to the maximal modulus of a nondegenerate eigenvalue defines the director $\hat{\mathbf{n}}$ of the system. The remaining two eigenvectors, which we denote $\hat{\mathbf{l}}$ and $\hat{\mathbf{m}}$, are the secondary directors. Hence, three orthogonal unit directors $\{\hat{\mathbf{n}}, \hat{\mathbf{l}}, \hat{\mathbf{m}} = \hat{\mathbf{n}} \times \hat{\mathbf{l}}\}$ and the associated eigenvalues are generally needed to account for local orientational properties of nematics, including, of course, N_{TB}.

The N_{TB} phase observed has a number of remarkable features. It looks uniform everywhere in space like cholesterics, with a temperature-dependent conical angle, $\theta_{\hat{\mathbf{n}}}$, ranging approximately between 9° and 30° (4, 19, 20). But, while the

Significance

The twist–bend nematic liquid crystalline phase is the fifth nematic structure recognized in nature [Chen D, et al. (2013) *Proc Natl Acad Sci USA* 110:15931–15936], and its stabilization is explained by assuming a coupling between polar and nematic orderings. It exhibits macroscopically chiral heliconical orientational order on the 10-nm scale and represents a unique example of spontaneous chiral symmetry breaking for a system of achiral molecules. Understanding how an external field affects the stability of this phase can shed further light on the origin of this induced twist and is of relevance to potential applications. Within the Landau–de Gennes theory we find that for compounds with positive anisotropy the helix unwinds to a polar nematic, however negative material anisotropy gives rise to a rich sequence of new nematic phases obtained via a mechanism of flattening the conical spiral.

Author contributions: G.P., L.L., and A.C. performed research, analyzed data, and wrote the paper.

The authors declare no conflict of interest.

This article is a PNAS Direct Submission. I.D. is a guest editor invited by the Editorial Board.

[1]To whom correspondence may be addressed. Email: grzegorz@th.if.uj.edu.pl, lech.longa@uj.edu.pl, or achrzano@usk.pk.edu.pl.

Published online October 11, 2018.

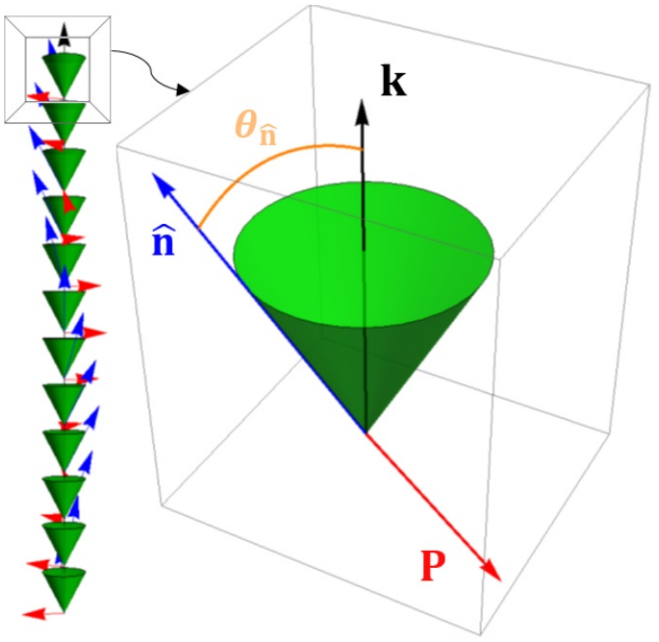

Fig. 1. Schematic representation of the nematic twist–bend structure. Right circular cone of conical angle $\theta_{\hat{\mathbf{n}}}$ shows the tilt between the director $\hat{\mathbf{n}}$ and the helical symmetry axis, parallel to the wave vector, $\mathbf{k}$. Red arrow represents polarization $\mathbf{P}$, where $\mathbf{P} \parallel \mathbf{k} \times \hat{\mathbf{n}}$; black arrow is the direction of $\mathbf{k}$.

cholesteric phase with its conical angle equal to a right angle ($\theta_{\hat{\mathbf{n}}} = \pi/2$) can homogeneously fill the space with a twist, the analogous arrangement for N_{TB} ($0 < \theta_{\hat{\mathbf{n}}} < \pi/2$) requires both bend and twist deformations to be present. X-ray diffraction experiments, sensitive to positional (3, 5) or orientational (21, 22) orderings, reveal no long-range positional order of molecular centers of mass (N_{TB} indeed remains a fully 3D liquid) but a 1D periodic order of molecular orientations. The helicoidal pitch length in N_{TB} is about 10 nm—that is, on the order of a few molecular lengths, which is about two orders of magnitude smaller than that typically found in cholesteric and blue phases (11). The N_{TB} phase is usually stabilized as a result of a first-order phase transition from the uniaxial nematic phase, but very recently a direct transition between N_{TB} and the isotropic phase has also been found (23, 24). Lack of molecular intrinsic chirality implies that coexisting domains of opposite handedness are formed and, consequently, the emergence of N_{TB} is related to a fundamental phenomenon—namely, the spontaneous chiral symmetry breaking.

While phenomenologically the spontaneous distortion of the N_{TB} and N_{SB} phases can effectively be explained as originating from the negative bend elasticity (12), the question of what microscopic/mesoscopic mechanism can be responsible for chiral symmetry breaking, especially the self-organization into N_{TB}, is still open and remains to be understood and explored. The issue has been addressed at the theoretical level in a series of papers (18, 25–33). Analysis shows that the molecules whose structure is sufficiently bent are a necessary requirement for the stabilization of N_{TB}, probably as a result of entropic, excluded volume interactions (25, 28). The molecules not only self-organize into a helical structure but also propagate long-range polar order of vanishing global polarization, transverse to the helical axis. For steric interactions, the polarity is a consequence of ordering of molecular bent cores (27, 28, 32, 33), and the other molecular interactions, such as between electrostatic dipoles, are probably less relevant for thermal stability of this phase. These conclusions seem in line with recent experimental observations (34–36).

A mesoscopic-level explanation of how molecular polarity of bent-core molecules can generate modulated polar nematic phases and, hence, effectively lower the bend elastic constant has been proposed to be due to the flexopolarization couplings, where derivatives of the alignment tensor (or of the director field) induce a net polarization (17, 18, 26, 29) (see supplemental material for ref. 37).

Model

We regard $\tilde{\mathbf{Q}}$ and $\tilde{\mathbf{P}}$ as dimensionless fields that characterize locally averaged orientational order of the bent-core molecules. A likely source of the polar order $\tilde{\mathbf{P}}(\tilde{\mathbf{r}})$ may be a sterically induced ordering due to specific bent-core molecular shapes, or it may be the electrostatic polarization due to molecular electric dipole moments (if present). On the other hand, the alignment tensor $\tilde{\mathbf{Q}}$ can be associated with the anisotropic part of macroscopic response functions of the bulk material (11). For example, it can be identified with the anisotropic part $\Delta\boldsymbol{\varepsilon}(\tilde{\mathbf{r}})$ of the dielectric (diamagnetic) susceptibility tensor $\boldsymbol{\varepsilon}(\tilde{\mathbf{r}})$: $\Delta\boldsymbol{\varepsilon} = \boldsymbol{\varepsilon} - \frac{1}{3}\mathrm{Tr}(\boldsymbol{\varepsilon})\mathbf{1}$, where $\mathbf{1}$ denotes the unit tensor and $\tilde{\mathbf{r}}$ stands for the position vector. Although the proportionality coefficient between $\Delta\boldsymbol{\varepsilon}$ and $\tilde{\mathbf{Q}}$ may be chosen at will, it is convenient to take (see, e.g., ref. 38)

$$\tilde{Q}_{\alpha\beta} = \Delta\varepsilon_{\alpha\beta}/\Delta\varepsilon_{max}, \qquad [2]$$

where $|\Delta\varepsilon_{max}|$ is the maximal anisotropy in the principal susceptibilities $\Delta\varepsilon$ ($\Delta\varepsilon = \varepsilon_{||} - \varepsilon_{\perp}$) that would be measured along ($\varepsilon_{||}$) or normal ($\varepsilon_{\perp}$) to the director in the perfectly ordered nematic phase. When $\Delta\varepsilon_{max} > 0$, the system has positive anisotropy and vice versa.

The minimal coupling model in $\tilde{\mathbf{Q}}(\tilde{\mathbf{r}})$ and $\tilde{\mathbf{P}}(\tilde{\mathbf{r}})$, which is able to account for N_{TB} ordering, is the LdeG free-energy expansion (17, 18, 39). It reads

$$\tilde{F} = \frac{1}{\tilde{V}}\int_{\tilde{V}} \tilde{f}\,\mathrm{d}^3\tilde{\mathbf{r}} = \frac{1}{\tilde{V}}\int_{\tilde{V}} \left(\tilde{f}_Q + \tilde{f}_P + \tilde{f}_{QP}\right)\mathrm{d}^3\tilde{\mathbf{r}}, \qquad [3]$$

where the free-energy densities, $\tilde{f}_X$, are constructed out of the fields X. The general form of $\tilde{f}_X$ for nonchiral liquid crystals is given by (17)

$$\tilde{f}_Q = a_Q\,\mathrm{Tr}(\tilde{\mathbf{Q}}^2) - b\,\mathrm{Tr}(\tilde{\mathbf{Q}}^3) + c\mathrm{Tr}(\tilde{\mathbf{Q}}^2)^2 + L_1(\boldsymbol{\nabla}\otimes\tilde{\mathbf{Q}})^2 + L_2(\boldsymbol{\nabla}\cdot\tilde{\mathbf{Q}})^2, \qquad [4]$$

$$\tilde{f}_P = a_P\,\tilde{\mathbf{P}}^2 + A_4(\tilde{\mathbf{P}}^2)^2 + b_P(\nabla\otimes\tilde{\mathbf{P}})^2 + A_c(\nabla\cdot\tilde{\mathbf{P}})^2, \qquad [5]$$

$$\tilde{f}_{QP} = -\varepsilon_P\tilde{\mathbf{P}}\cdot(\nabla\cdot\tilde{\mathbf{Q}}) - \Lambda_{QP}\tilde{P}_\alpha\tilde{Q}_{\alpha\beta}\tilde{P}_\beta. \qquad [6]$$

Here, b, c, L_1, L_2, A_4, b_P, A_c, ε_P, and Λ_{QP} are temperature-independent constitutive parameters, $(\boldsymbol{\nabla}\otimes\tilde{\mathbf{Q}})^2 = (\partial_i\tilde{Q}_{jk})(\partial_i\tilde{Q}_{jk})$, $(\boldsymbol{\nabla}\cdot\tilde{\mathbf{Q}})^2 = (\partial_i\tilde{Q}_{ik})(\partial_j\tilde{Q}_{jk})$, and $(\nabla\otimes\tilde{\mathbf{P}})^2 = (\partial_i\tilde{P}_j)(\partial_i\tilde{P}_j)$; repeated indices are summed over.

As always in Landau theory, the temperatures $a_Q = a_{0Q}(T - T^*)$ and $a_P = a_{0P}(T - T_P)$ are connected with the absolute temperature T of the system; T^* is the spinodal for a first-order phase transition from the isotropic phase to an orientationally ordered phase or transition temperature otherwise; T_P is the transition temperature to a polar phase of $\tilde{\mathbf{Q}} = 0$ and $\tilde{\mathbf{P}} \neq 0$. We take $a_P > 0$, which eliminates spontaneous polar order ($\tilde{\mathbf{P}} \neq 0$) in the absence of $\tilde{\mathbf{Q}}$. Since $a_{0P} > 0$, $a_{0Q} > 0$, $T^* > T_P$, and $T > T_P$, any straight line in the $\{a_Q, a_P\}$ plane with positive slope and

negative a_Q-intercept represents a permissible physical system with no polar order for $\tilde{\mathbf{Q}}=0$. In the remaining parts of the free-energy density, A_c is the strength of the longitudinal contribution from the steric polarization, ε_P is the strength of flexopolarization, and Λ_{QP} is the strength of direct coupling between $\tilde{\mathbf{Q}}$ and $\tilde{\mathbf{P}}$ fields. For thermodynamic stability of $\tilde{f}$ against an unlimited growth of $\tilde{\mathbf{Q}}(\tilde{\mathbf{r}})$ and $\tilde{\mathbf{P}}(\tilde{\mathbf{r}})$, it is mandatory that $c>0$, $L_1>0$, $L_1+\frac{2}{3}L_2>0$, $A_4>0$, and $b_P+A_c>0$. Note that Eqs. **4–6** contain all symmetry-allowed invariants up to fourth order in $\tilde{\mathbf{Q}}$ and $\tilde{\mathbf{P}}$ and include for the quadratic part those involving first-order spatial derivatives of $\tilde{\mathbf{Q}}$ and $\tilde{\mathbf{P}}$. Higher order elastic and bulk contributions, which could be significant (see ref. 39), will not be considered here. When the flexopolarization coupling becomes strong enough (18),

$$4\,L_2-\varepsilon_P^2/a_P\le -6\,L_1, \qquad [7]$$

the uniform nematic phase can no longer be stable, and a modulated polar order is formed. In addition to N_{TB} and N_{SB}, the theory (Eq. **3**) predicts the existence of two further 1D modulated nonchiral, polar nematic phases with transverse and longitudinal polarization being modulated along just one direction (18). But it is important to observe that the flexopolarization term alone ($\varepsilon_P\neq 0$) is not sufficient to bring about spontaneous chiral symmetry breaking. It needs to be accompanied, at least, by the nonvanishing Λ_{QP}-coupling ($\Lambda_{QP}\neq 0$) in $\tilde{F}$. The nonvanishing Λ_{QP} is also needed for a proper explanation of the fluctuation modes in N_{TB}, as suggested by recent light-scattering experiments (40).

Alternative mesoscopic scenarios pertaining to the stability of N_{TB}, like these involving couplings between the alignment tensor and higher rank (octupolar) order parameters, have also been proposed (41–47). With the recent discovery of a bent-core material exhibiting anomalously low twist and bend elastic constants (48), this indicates that the theoretical studies of mechanism(s) responsible for observed spontaneous chiral symmetry breaking are still in their initial stage, and further research is needed to provide understanding of the stability of N_{TB}. One promising direction, which we would like to follow here, is a systematic analysis of how properties of N_{TB} can change in the presence of external stimuli, such as electric or magnetic fields, surface anchoring, photochemically driven trans cis isomerization, etc. Such analysis can also be important in seeking future practical applications of this new phase.

In the case of modulated nematics, their response to an external field can become highly nontrivial (11, 49). In cholesterics, for example, it is possible to unwind the orientational spiral through an intermediate heliconical structure (50, 51), both for bulk sample (52) and in confined geometry (53, 54). A more comprehensible, field-induced modification of cholesterics involves reorientation of the helical axis (11) or changing the pitch (55). Similar effects can be expected for N_{TB}, although recent magnetic field experiments (56, 57) show only depletion of the $N-N_{\mathrm{TB}}$ transition temperature, without a noticeable distortion of the structure. So far, theoretical attempts to characterize the interaction of N_{TB} with the field have been made on the basis of the Frank elastic theory (58–60).

The purpose of this paper is to study, in a systematic way, a response of the bulk N_{TB} phase to the external fields (electric, magnetic) within the frame of the LdeG free energy (Eqs. **3–6**). As N_{TB} is expected for nonchiral bent-shaped molecules, with and without electric dipoles, we assume that stability of this phase is driven primarily by excluded-volume, entropic interactions (28). We consider the LdeG free energy (Eq. **3**) supplemented by the dielectric (diamagnetic) term, $\tilde{F}_E$ ($\tilde{F}\to\tilde{F}+\tilde{F}_E$, $\tilde{F}_E=\frac{1}{\tilde{V}}\int_{\tilde{V}}\tilde{f}_E\,\mathrm{d}^3\tilde{\mathbf{r}}$), where (11, 38)

$$\tilde{f}_E=-\frac{1}{2}\varepsilon_0\tilde{E}_\alpha\Delta\varepsilon_{\alpha\beta}\tilde{E}_\beta=-\frac{1}{2}\varepsilon_0\Delta\varepsilon_{max}\tilde{E}^2\hat{e}_\alpha\tilde{Q}_{\alpha\beta}(\tilde{\mathbf{r}})\hat{e}_\beta. \qquad [8]$$

Here, $\tilde{E}^2=\tilde{E}_\alpha\tilde{E}_\alpha$, and $\hat{\mathbf{e}}$ is the unit vector collinear with $\tilde{\mathbf{E}}$; ε_0 is the permittivity constant of the vacuum for an applied electric field and inverse of the permeability of vacuum ($\varepsilon_0\to\mu_0^{-1}$) for a magnetic field. Note that we omitted in Eq. **8** any coupling with the field that is independent of orientation. We think that the dielectric (diamagnetic) term should dominate, at least for sufficiently strong fields, and disregard a possible direct interaction between the dipole moments and the field.

It is now useful to rewrite Eq. **3** in terms of reduced (dimensionless) quantities, which reveals the redundancy of four parameters in the expressions (Eqs. **4–6**) and allows us to set them to one from the start (17, 18, 39, 61). We introduce the reduced quantities F, f, $\mathbf{r}$, $\mathbf{Q}$, $\mathbf{P}$, t_Q, ρ, t_P, a_c, a_d, e_P, λ, $\Delta\epsilon\,E^2$, and $\mathbf{k}$ using equations

$$\tilde{F}=\frac{b^4}{c^3}\,F\quad\left(\tilde{f}=\frac{b^4}{c^3}\,f\right),\quad \tilde{\mathbf{r}}=\frac{2\sqrt{c\,L_1}}{b}\mathbf{r},\quad \tilde{\mathbf{Q}}=\frac{b}{c}\mathbf{Q}, \qquad [9]$$

$$\tilde{\mathbf{P}}=\frac{b\sqrt{L_1}}{c\sqrt{b_P}}\,\mathbf{P},\quad a_Q=\frac{b^2}{4c}t_Q,\quad L_2=L_1\,\rho, \qquad [10]$$

$$a_P=\frac{b^2 b_P}{4\,c\,L_1}\,t_P,\quad A_c=b_P\,a_c,\quad A_4=\frac{c\,b_P^2}{L_1^2}\,a_d, \qquad [11]$$

$$\varepsilon_P=\frac{b\,\sqrt{b_P}}{2\,\sqrt{c}}\,e_P,\quad \Lambda_{QP}=\frac{b\,b_P}{L_1}\,\lambda, \qquad [12]$$

$$\tilde{E}^2=\frac{2\,b^3}{c^2\,\varepsilon_0\,\Delta\varepsilon_{\max}}\,(\Delta\epsilon\,E^2),\quad \tilde{\mathbf{k}}=\frac{b}{2\sqrt{c\,L_1}}\,\mathbf{k}, \qquad [13]$$

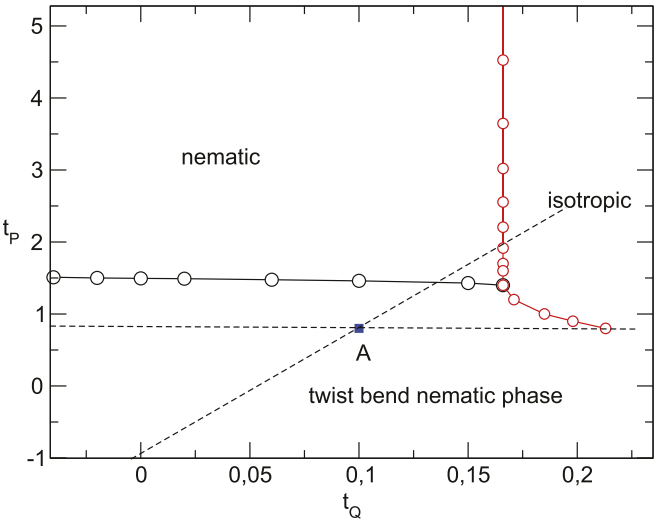

Fig. 2. Schematic phase diagram involving only isotropic, nematic, and nematic twist–bend phases obtained within the relaxation method. Given also is an exemplary reference N_{TB} state (blue point A) for which a detailed response to the external field has been found. Any physical system is represented by a straight line of the positive tangent and negative t_Q intercept, passing through a point, A—that is, lying between the two limiting dashed lines shown. Note that the generic system represented by A gives all sequences of phases with stable N_{TB} observed experimentally—namely, $I-N-N_{\mathrm{TB}}$ and a direct $I-N_{\mathrm{TB}}$. Each allowed straight line is parameterized by the temperature T according to linear relations between t_Q and a_Q and between t_P and a_P (Eqs. **10** and **11**). Detailed calculations of the field effect on the N_{TB} phase are carried out for $\rho=1$, $a_c=2$,$e_P=-4$, $a_d=1$, and $\lambda=-1/2$.

PHYSICS

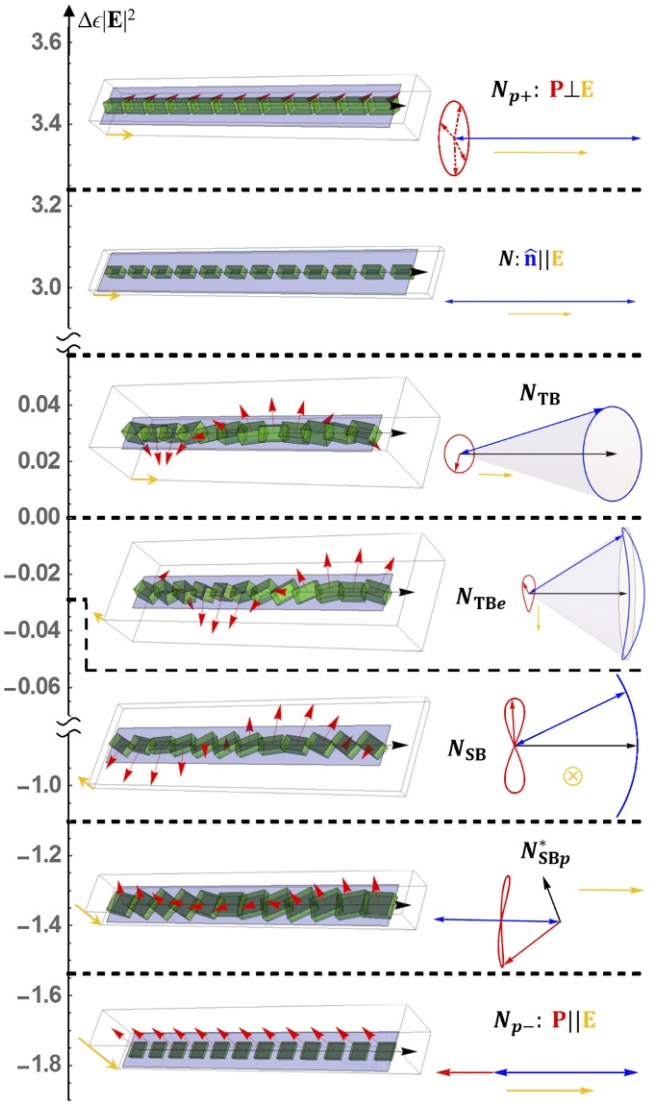

Fig. 3. Transformation of N_{TB} with an applied external field. The dashed lines correspond to the values of $\Delta\epsilon|\mathbf{E}|^2$ that lead to phase transformation; yellow arrows are directions of the field **E** in each of the structures. Red arrowheads represent the polarization vector **P**, and the black arrowhead is the direction of the wave vector **k**. Lengths of cuboid edges are proportional to the eigenvalues of $\mathbf{Q}+c\mathbf{I}$, where **I** is the unit matrix and c is a constant, such that the isotropic state is represented by a cube. Directions of cuboid edges, equivalent to principal axes of **Q**, are along the directors, where the main principal axis associated with the maximal nondegenerated eigenvalue of **Q** is parallel to $\hat{\mathbf{n}}$. The secondary directors $\hat{\mathbf{m}}$ and $\hat{\mathbf{l}}$ are parallel to the remaining two cuboid edges, with the rule that $\hat{\mathbf{m}}=\hat{\mathbf{n}}\times\hat{\mathbf{l}}$ is associated with the next-to-maximal eigenvalue. Rightmost are schematic representations of the structures with the main director $\hat{\mathbf{n}}$ shown as the blue double-arrow. Blue curves depict successive, field-induced deformations of the N_{TB} cone of $\hat{\mathbf{n}}$, while **P** follows the red curves. Note that the N_{p_+} phase ($\Delta\epsilon>0$) is uniaxial with **P** degenerated on a circle, perpendicular to the director. In $N^*_{\mathrm{SB}p}$, the main director is fixed in space, while the secondary directors are responsible for the in-plane splay–bend deformations. The polarity of this phase induces chiral order. The N_{p_-} phase is a polar uniaxial nematic with polarization parallel to $\hat{\mathbf{n}}$.

where $\tilde{\mathbf{k}}$ is the physical wavevector. Eqs. **3–6** and **8** then become

$$F\equiv F[\mathbf{Q},\mathbf{P}]=\frac{1}{V}\int_V (f_Q+f_P+f_{QP}+f_E)\mathrm{d}^3\mathbf{r}, \qquad [14]$$

where

$$f_Q=\frac{1}{4}\left[t_Q\,\mathrm{Tr}(\mathbf{Q}^2)+(\boldsymbol{\nabla}\otimes\mathbf{Q})^2+\rho(\boldsymbol{\nabla}\cdot\mathbf{Q})^2\right] -\mathrm{Tr}(\mathbf{Q}^3)+\mathrm{Tr}(\mathbf{Q}^2)^2, \qquad [15]$$

$$f_P=\frac{1}{4}\left[t_P\,\mathbf{P}^2+(\boldsymbol{\nabla}\otimes\mathbf{P})^2+a_c(\boldsymbol{\nabla}\cdot\mathbf{P})^2\right]+a_d(\mathbf{P}^2)^2, \qquad [16]$$

$$f_{QP}=-\frac{1}{4}e_P\mathbf{P}\cdot(\nabla\cdot Q)-\lambda P_\alpha Q_{\alpha\beta}P_\beta, \qquad [17]$$

$$f_E=-\Delta\epsilon E^2\hat{e}_\alpha Q_{\alpha\beta}(\mathbf{r})\hat{e}_\beta. \qquad [18]$$

We explore the absolute stability of the N_{TB} phase for the model (Eqs. **14–18**) by limiting to a family of all One-Dimensional Modulated Nematic Structures (ODMNS), periodic at most in one spatial direction (18). Starting with the N_{TB} phase, which is stable within the ODMNS family for the vanishing field, we identify free-energy minimizers for the nonzero field. A full account of the electric field response, with terms quadratic and linear in the field, will be presented elsewhere.

All possible ODMNS structures can be parameterized with the aid of the plane wave expansions of $\mathbf{Q}(\mathbf{r})$ and $\mathbf{P}(\mathbf{r})$ (17, 18): $\mathbf{Q}(\mathbf{r})=\sum_n\sum_{m=-2}^{2}Q_m(n)\exp(\mathrm{i}\,nk\,\hat{\mathbf{z}}\cdot\mathbf{r})\,\mathbf{e}^{[2]}_{m,\hat{\mathbf{z}}}$, $\mathbf{P}(\mathbf{r})=\sum_n\sum_{m=-1}^{1}P_m(n)\exp(\mathrm{i}\,nk\,\hat{\mathbf{z}}\cdot\mathbf{r})\,\mathbf{e}^{[1]}_{m,\hat{\mathbf{z}}}$, where $nk\hat{\mathbf{z}}=\mathbf{k}$ are the wave vectors ($n=0,\pm1,\ldots$), $Q_m(n)$ and $P_m(n)$ are the unknown amplitudes found from the minimization of the free-energy expansion, and $\mathbf{e}^{[L]}_{m,\hat{\mathbf{z}}}$ and $m=0,\pm1,\pm L$ are the spin $L=1,2$ spherical tensors represented in a laboratory coordinate system with quantization axis along the $\hat{\mathbf{z}}$ direction. The selection of k, $Q_m(n)$, and $P_m(n)$ is fixed by minimization of F, supplemented by the bifurcation analysis (see supplemental material for ref. 37) (61, 62). Only $n=0$ terms couple to a uniform external field in Eq. **18**, giving

$$f_E=-\Delta\epsilon E^2\left\{\sin^2(\theta)\,[x_{20}\cos(2\phi)-y_{20}\sin(2\phi)]+\sin(2\theta)\right. \left.[y_{10}\sin(\phi)-x_{10}\cos(\phi)]+x_{00}\,[3\cos(2\theta)+1]/(2\sqrt{6})\right\}, \qquad [19]$$

where $\mathbf{E}=E[\cos(\phi)\sin(\theta),\sin(\phi)\sin(\theta),\cos(\theta)]$ is the external field expressed in the laboratory system of the frame and where $\mathfrak{Re}\,Q_m(n)=x_{mn}$ and $\mathfrak{Im}\,Q_m(n)=y_{mn}$. The relative orientation of **Q** and **E**, parameterized by θ and ϕ, is found by minimization of F.

Our starting point is the identification of homogeneous structures of wave vector k that can be constructed out of **Q** and **P**, among which should be the N_{TB} phase. The spatial homogeneity of a structure implies that $\forall z$ the tensors $\mathbf{Q}(z)$ and, say, $\mathbf{Q}(0)$ for $z=0$ are connected by a rotation. More specifically, $\mathbf{Q}(z)$ can be obtained from $\mathbf{Q}(0)$ by rotating through the angle kz about $\hat{\mathbf{z}}$: $\mathcal{R}_{\hat{z}}(\pm kz)\mathbf{Q}(0)=Q_\pm(z)$, where $\pm$ stands for right- and left-handed heliconical structure. Likewise, through the same rotation, $\mathbf{P}(0)$ is transformed into $\mathbf{P}(z)$: $\mathcal{R}_{\hat{z}}(\pm kz)\mathbf{P}(0)=\mathbf{P}_\pm(z)$. The structures fulfilling the above conditions have a unique

Table 1. Critical values of $\Delta\epsilon E^2$ at field-induced phase transitions for the reference state A of Fig. 2

Transition	$\Delta\epsilon E^2$
$N-N_{p_+}$	3.24
$N_{\mathrm{TB}}-N$	0.058
$N_{\mathrm{TB}}-N_{\mathrm{TBe}}$	−0
$N_{\mathrm{TBe}}-N_{\mathrm{SB}}$	−0.029
$N_{\mathrm{SB}}-N^*_{\mathrm{SB}p}$	−1.10
$N^*_{\mathrm{SB}p}-N_{p_-}$	−1.54

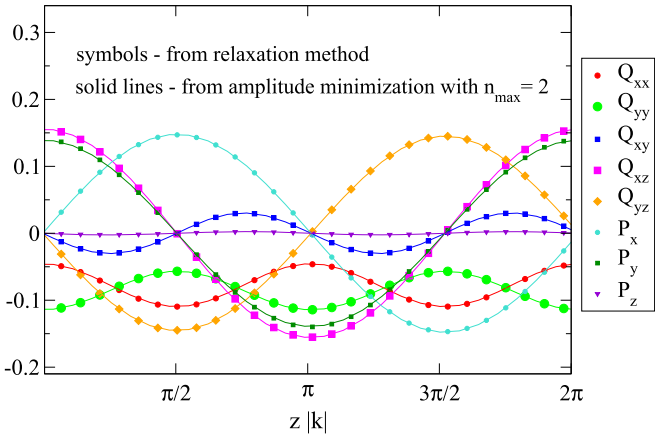

Fig. 4. **Q** and **P** fields obtained for N_{TB} from the relaxation method (symbols) and from the free-energy minimization with respect to the Fourier amplitudes for $n_{max}=2$ (lines) for $\Delta\epsilon E^2=0.0025$ (where $|\mathbf{k}|\approx 0.45$; see Fig. 7).

form given by the terms of $|n|\le 2$ in the expansions of **Q** and **P**—namely,

$$\mathbf{Q}_{\pm}(z)=Q_0(0)\mathbf{e}^{[2]}_{0,\hat{\mathbf{z}}}+\sum_{m=1}^{2}\left[Q_{\pm m}(m)\mathbf{e}^{[2]}_{\pm m,\hat{\mathbf{z}}}e^{\pm imkz}+c.c\right], \quad [20]$$

$$\mathbf{P}_{\pm}(z)=P_0(0)\mathbf{e}^{[1]}_{0,\hat{\mathbf{z}}}+\left[P_{\pm 1}(1)\mathbf{e}^{[1]}_{\pm 1,\hat{\mathbf{z}}}e^{\pm ikz}+c.c\right]. \quad [21]$$

For example, the explicit formulas for $\mathbf{Q}_+$ and $\mathbf{P}_+$ read

$$\mathbf{Q}_{+}(z)=\begin{bmatrix} c_2(z)r_2-\frac{x_{00}}{\sqrt{6}} & -s_2(z)r_2 & -c_1(z)r_1 \\ -s_2(z)r_2 & -c_2(z)r_2-\frac{x_{00}}{\sqrt{6}} & s_1(z)r_1 \\ -c_1(z)r_1 & s_1(z)r_1 & \sqrt{\frac{2}{3}}x_{00}\end{bmatrix}, \quad [22]$$

$$\mathbf{P}(z)\equiv\mathbf{P}_{+}(z)=\begin{bmatrix} -\sqrt{2}p_1\cos(kz+\phi_p) \\ \sqrt{2}p_1\sin(kz+\phi_p) \\ v_{00}\end{bmatrix}. \quad [23]$$

Here, $\mathbf{Q}_+(z)\equiv\mathbf{Q}(z)$, $c_i(z)=\cos(ikz+\phi_i)$, $s_i(z)=\sin(ikz+\phi_i)$, $r_i\cos(\phi_i)=x_{ii}$, $r_i\sin(\phi_i)=y_{ii}$ $(r_i\ge 0)$, $p_1\cos(\phi_p)=v_{11}$, and $p_1\sin(\phi_p)=z_{11}$ $(p_1\ge 0)$, where $v_{ij}=\mathfrak{Re}P_i(j)$, $z_{ij}=\mathfrak{Im}P_i(j)$, and as previously, $x_{ij}=\mathfrak{Re}Q_i(j)$ and $y_{ij}=\mathfrak{Im}Q_i(j)$. Note that one of the three phases ϕ_i $(i=1,2,p)$ is the Goldstone mode and can be eliminated, which expresses the freedom of choosing the origin of the laboratory system of the frame. In what follows we set $\phi_1=0$. Hence, a family of all homogeneous (polar) helical nematic mesophases, structurally linked with the uniaxial nematic phase (N), can be parameterized unambiguously using at most eight parameters (including the k vector). The x_{00} terms in Eq. **22** represent the reference N phase with the director along $\hat{\mathbf{z}}$, while v_{00} indicates that each of the structures can also be globally polar. As the systems we study are nonchiral, the spontaneous chiral symmetry breaking means that domains representing opposite chiralities have the same free energy, $F[\mathbf{Q}_+,\mathbf{P}_+]=F[\mathbf{Q}_-,\mathbf{P}_-]$, and that they are formed with equal probability (ambidextrous chirality).

Setting $r_1=0$ in Eq. **22** gives the cholesteric phase of the conical angle $\theta_{\hat{\mathbf{n}}}=\pi/2$ (Eq. **1**), while the simplest parameterization of the N_{TB} phases is obtained by neglecting terms with $m=2$ $(r_2=0)$ in Eq. **22**. In this simplified case, the conical angle is given by

$$\cos(\theta_{\hat{\mathbf{n}}})=\frac{\sqrt{3\chi^2+8}+\sqrt{3}\chi}{\sqrt{2}\sqrt{3\chi^2+\sqrt{9\chi^2+24}\chi+8}}, \quad [24]$$

where $\chi=x_{00}/r_1$. Note that $0\le\theta_{\hat{\mathbf{n}}}\le\pi/4$ for a prolate uniaxial nematic background $(x_{00}\ge 0)$, while the oblate case $(x_{00}\le 0)$ yields $\pi/2\ge\theta_{\hat{\mathbf{n}}}\ge\pi/4$. The general case of N_{TB} with $r_2\neq 0$ allows for a fine control of biaxiality and of the conical angle. The former can be measured by the coordinate-independent normalized parameter w (11, 39, 63),

$$-1\le w(\mathbf{Q})=\sqrt{6}\ Tr(\mathbf{Q}^3)/\left[Tr(\mathbf{Q}^2)\right]^{\frac{3}{2}}\le 1, \quad [25]$$

which yields $w=1$ $(w=-1)$ for the locally uniaxial prolate (oblate) order, where two out of the three eigenvalues of **Q** are equal. The biaxial order with three eigenvalues of **Q** being different is characterized by $|w|<1$. The maximal biaxiality is accomplished for $w=0$ when one eigenvalue of **Q** vanishes (for more details, see figure 1 in ref. 63). In particular, for N_{TB}, the parameter w is given by

$$w=\frac{\chi\left(-6\tau^2+\chi^2+3\right)+3\sqrt{6}\,\tau\cos(\phi_2)}{(2\tau^2+\chi^2+2)^{3/2}}, \quad [26]$$

where $\tau=r_2/r_1$. Note that w in Eq. **26** is k-independent, expressing the fact that z dependence of **Q** in Eq. **22** is generated by a rotation. This means that N_{TB} is biaxial, and in the limit of $k\to 0$, we get the fourth of homogeneous nematic structures accounted for by Eq. **22**—namely, the biaxial nematic.

Each of the structures identified so far can be polar (Eq. **23**). For $k\neq 0$, the polarization can acquire the long-range periodic component in the $x-y$ plane $(p_1\neq 0)$, which is perpendicular to $\hat{\mathbf{z}}$, and/or global macroscopic polarization $(v_{00}\neq 0)$, parallel to $\hat{\mathbf{z}}$. Interestingly, the N_{TB} phase given by Eqs. **22** and **23** with $v_{00}=0$ can be the global minimizer within the ODMNS class. The sufficient condition for the free-energy parameters can be derived using the bifurcation analysis (see supplemental material for ref. 37) with uniaxial nematic $(x_{00}\neq 0)$ as a reference state. It reads

$$\frac{-4\,t_P}{1+\sqrt{1-16\,t_Q/3}}<\lambda<\frac{e_P^2-4(2+\rho)t_P}{(\rho+2)\left(1+\sqrt{1-16\,t_Q/3}\right)}, \quad [27]$$

which is valid when the following additional constraints are fulfilled: $e_P\neq 0$, $t_Q<\frac{1}{6}$, $\rho>-\frac{3}{2}$, and $t_P>0$.

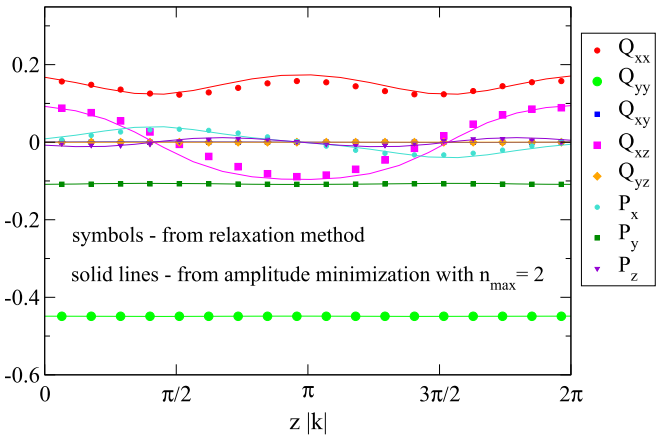

Fig. 5. **Q** and **P** fields obtained for $N^*_{\mathrm{SB}p}$ from the relaxation method (symbols) and from the free-energy minimization with respect to the Fourier amplitudes for $n_{max}=2$ (lines) for $\Delta\epsilon E^2=-1.3225$ (where $(|\mathbf{k}|\approx 0.20$; see Fig. 7).

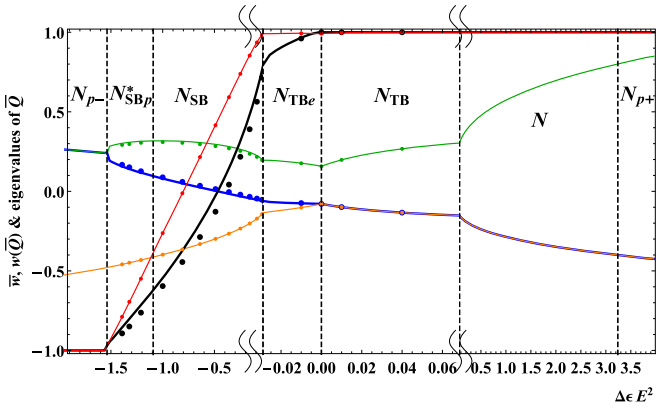

Fig. 6. Various observables averaged over one period from the relaxation method (points) and from the free-energy minimization with respect to the Fourier amplitudes for $n_{max} = 2$ (lines). Eigenvalues of $\overline{Q}$ are given in green (along wave vector), orange (for negative anisotropy, it is along the direction of the external field), and blue. The biaxiality parameter, given by Eq. **25**, is plotted in red for $\overline{w}$ and in black for $w(\overline{Q})$.

Results

In seeking a globally stable structure among ODMNS, we need to take into account both homogeneous and inhomogeneous trial states given by the plane wave expansions of **Q** and **P**. The complexity of the ODMNS minimization depends on the number of amplitudes used in this expansion, which is controlled by the maximal value n_{max} of $|n|$ in the set $\{k, Q_m(n), P_m(n),\ n = 0, \pm 1, \ldots, \pm n_{max}\}$. As it turns out, the $n_{max} = 1$ approximation with 25 real, variational parameters is not sufficient to qualitatively reproduce structural changes as experienced by $N_{\rm TB}$ due to an applied external field. To obtain credible results, the following strategy has proved to work. In the first step, we perform the free-energy minimization with $n_{max} = 2$. Then, the identified structures serve in the next step as initial states in seeking for the improved free-energy minimum, where the relaxation method for 1D periodic structures is being used for the bulk sample. A short summary of this typical method is given below.

More specifically, we consider the bulk $N_{\rm TB}$ sample of thickness Λ with free boundary conditions at $z = 0$ and $z = \Lambda$ ($0 \le z \le \Lambda$), where Λ is much larger than the period of the structure. Then, we divide the sample in the z direction into N equal intervals and approximate the fields $\mathbf{Q}(z)$ and $\mathbf{P}(z)$ at nodes z_i taken in the middle of each interval i. For the derivatives of the fields, we use the central difference approximation

$$\partial \mathbf{X}(z)/\partial z|_{z=z_i} = [\mathbf{X}(z_{i+1}) - \mathbf{X}(z_{i-1})]/2\delta, \qquad [28]$$

where δ is the distance between the two neighboring nodes and where $\mathbf{X} = \mathbf{Q}(z)$ or $\mathbf{P}(z)$. After these preparations are done, the volume integral in F is discretized in a standard way using a simple trapezoidal rule, with the node variables $\{\mathbf{X}\} \equiv \{\mathbf{Q}(z_i), \mathbf{P}(z_i),\ i = 1, \ldots 8N\}$ playing the role of variational parameters.

The relaxation method for the discretized free energy determines $\{\mathbf{X}\}$ with the following iterative formula:

$$\mathbf{X}^{(n+1)}(z_i) - \mathbf{X}^{(n)}(z_i) = -\gamma\ \partial F/\partial \mathbf{X}(z_i)|_{\mathbf{X}(z_i)=\mathbf{X}^{(n)}(z_i)}, \qquad [29]$$

where the superscript (n) enumerates the values of $\{\mathbf{X}(z_i)\}$ obtained in successive iterations and γ is the relaxation parameter. For the convergent iterations, we typically used $\gamma = 0.005$ and $N = 4000$, but generally, the choice of γ is not important, unless numerical instabilities occur. Occasionally, we doubled the number of nodes to see the influence on the accuracy of the free energy. The iteration was initialized with $\mathbf{X}^{(1)}(z_i) \equiv \mathbf{X}(z_i)$ using analytic expressions obtained from the Fourier amplitude minimization for $n_{max} = 2$ for the case without the external field. The corresponding periodicity $(2\pi/k)$ of $N_{\rm TB}$ was used to fix Λ. Once initialized, the system (Eq. **29**) was solved iteratively until self-consistency with the required accuracy was achieved. We used very large bulk samples of $\Lambda \approx 260\pi/k$ for which the structure close to the midplane ($z \approx \Lambda/2$) was insensitive to the ordering near boundaries. The next step was the equilibration of the k vector for the **X** fields evolved during the relaxation process. The method we used is described in detail in refs. 64 and 65 and is based on the observation that under distance rescaling, $z \to z/\kappa$ the free energy is a general quadratic function of κ, with coefficients that are κ-independent. Thus, the scaling factor, κ^*, obtained by the subsequent minimization of the free energy, gives the improved wave vector, $\kappa^* k$, for the approximate **X** fields that are obtained from relaxation. Effectively, it amounts in rescaling the distance between the nodes: $\delta \to \delta' = \delta/\kappa^*$ of the relaxed fields. The relaxation procedure is then repeated with the new δ' and followed by a new rescaling. The process continued until $\kappa^* \cong 1$. To find solutions for the cases with the electric field, we repeated the above procedure using as the initial condition the solution from the step with a smaller field. A typical (generic) $N_{\rm TB}$ reference state taken for detailed field analysis is shown in Fig. 2, point A.

Results of the numerical analysis are illustrated for the case when $\rho = 1$, $a_c = 2$, $e_P = -4$, $a_d = 1$, $\lambda = -1/2$, $t_Q = 1/10$, and $t_P = 8/10$, where without the external field the heliconical structure is most stable among ODMNS, isotropic, uniaxial, and biaxial nematics. Depending on the strength of the field and the sign of the material anisotropy, both controlled by the single model parameter $\Delta\epsilon E^2$ in Eq. **18**, the $N_{\rm TB}$ structure can evolve, as shown in Fig. 3. For the case of positive material anisotropy ($\Delta\epsilon E^2 > 0$), the minimum is realized for $\mathbf{E} || \hat{\mathbf{k}}$, while for negative anisotropy ($\Delta\epsilon E^2 < 0$) the minimum occurs when $\mathbf{E} \perp \hat{\mathbf{k}}$. Furthermore, in the positive anisotropy case, the $N_{\rm TB}$ phase unwinds to the uniaxial nematic with the director parallel to the external field. Further increase of the field results in

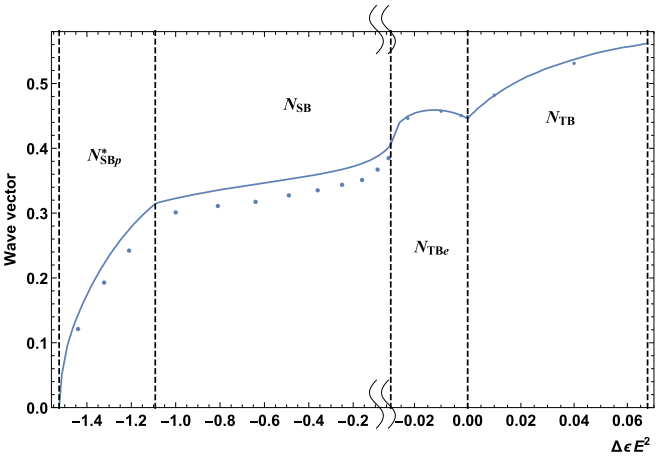

Fig. 7. Wave vector as a function of the external field for ODMNS presented in Fig. 3. As previously, points are from the relaxation method, and the line is the outcome of the free-energy minimization with respect to the Fourier amplitudes for $n_{max} = 2$. Dimensionless wave vector for the zero field case ($k(E = 0) \approx 0.446$) when matched to typical experimental data of $k_0 = 2\pi/10[nm^{-1}] \approx 0.628[nm^{-1}]$ fixes the scale factor in Eq. **13**, giving a partial link between the theory and experiment. The procedure reduces the number of model parameters in Eq. **13**, but a full comparison with the experiment would require further experimental data as discussed in the last chapter.

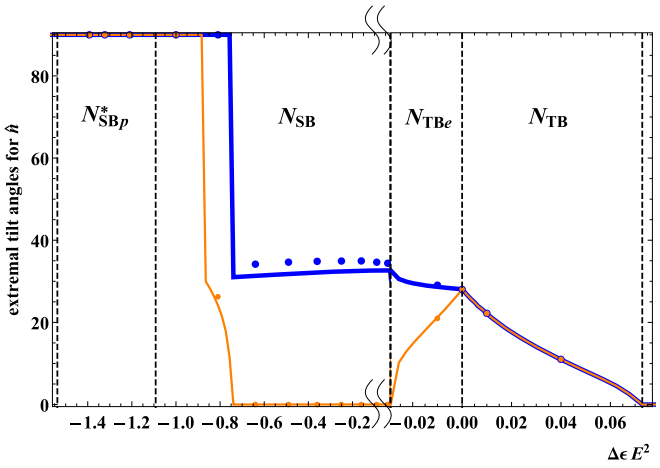

Fig. 8. Minimal (orange) and maximal (blue) values of angle between **k** and $\hat{\mathbf{n}}$. As previously, points are from the relaxation method, and lines are outcomes of the free-energy minimization with respect to the Fourier amplitudes for $n_{max} = 2$.

stabilization of a polar nematic (N_{p_+}), where the polarization vector is arbitrarily orientated in the plane perpendicular to $\hat{\mathbf{n}}$. The case of negative anisotropy modifies instantly the modulation of the main director in the N_{TB} phase, which is now precessing on the elliptic cone around $\hat{\mathbf{k}}$, shown in gray in Fig. 3. We denote this new structure as $N_{\mathrm{TB}e}$. Stronger fields ($\mathbf{E}\perp\hat{\mathbf{k}}$) make the elliptic cone narrower, and finally N_{SB} is stabilized, where the cone becomes degenerated to an isosceles triangle (i.e., $\hat{\mathbf{n}}$ becomes confined to a circular arc) and **P** lies in the plane of splay–bend modulations. With larger fields, the in-plane modulations diminish, and **P** acquires an out-of-plane uniform component along the field. This is a new chiral structure, denoted $N^*_{\mathrm{SB}p}$, where the modulation of the main director is replaced by splay–bend modulations of the secondary directors. For even stronger fields, this phase transforms to a polar nematic (N_{p_-}) with polarization parallel to the field and $\hat{\mathbf{n}}$. Values of the dimensionless field parameter that induces phase transitions are gathered in Table 1. Quantitatively, phases are described by the amplitudes $Q_m(n)$ and $P_m(n)$ or equivalently by their real and imaginary parts, which we denote $x_{ij} = \mathfrak{Re}\, Q_i(j)$, $y_{ij} = \mathfrak{Im}\, Q_i(j)$, $v_{ij} = \mathfrak{Re}\, P_i(j)$, and $z_{ij} = \mathfrak{Im}\, P_i(j)$. Additionally, each structure is characterized by the wave vector k. For stable ODMNS with $n_{max} = 2$, the sets of nonzero parameters are as follows: $\{y_{11}, y_{22}, x_{00}, x_{11}, x_{22}, z_{11}, v_{11}\}$ for N_{TB}; as in N_{TB} and $\{y_{-22}, y_{-11}, y_{02}, x_{-22}, x_{-11}, x_{02}, x_{20}, z_{-11}, z_{02}, v_{-11}, v_{02}\}$ for $N_{\mathrm{TB}e}$; as in $N_{\mathrm{TB}e}$, provided that the following constrains are fulfilled, $\{|y_{-22}| = |y_{22}|,\ |y_{-11}| = |y_{11}|,\ |x_{-22}| = |x_{22}|,\ |x_{-11}| = |x_{11}|, |z_{-11}| = |z_{11}|, |v_{-11}| = |v_{11}|\}$, for N_{SB}; and as in N_{SB} in union with $\{|y_{-21}| = |y_{-12}|, |y_{12}| = |y_{21}|, |x_{-21}| = |x_{-12}|, |x_{12}| = |x_{21}|, |z_{-12}| = |z_{12}|, z_{10}, |v_{-12}| = |v_{12}|\}$ for $N^*_{\mathrm{SB}p}$. A typical outcome of the standard relaxation procedure for stable structures and how it compares with the amplitude minimization for $n_{max} = 2$ is illustrated in Figs. 4–10. Note that both the $n_{max} = 2$ amplitude minimization and the relaxation results agree quantitatively, indicating that the approximation of $n_{max} = 2$ is sufficient to obtain the basic features of the phases studied. Taking $n_{max} = 1$ leads to qualitatively inconsistent results, which means that two Fourier harmonics of wave vectors **k** and 2**k** are required to account for structural properties of N_{TB} and of the related structures.

To gain an insight into fine structure of stable phases, we plot characteristic observables for each of them in Figs. 6–10. First, we present the behavior of eigenvalues for $\boldsymbol{Q}(z)$ averaged over one period ($\overline{\boldsymbol{Q}}$) (Fig. 6), which is what can effectively be measured in experiments. Please note that homogeneous nematics and N_{TB} (averaged over one period) are uniaxial, as two eigenvalues of $\overline{\boldsymbol{Q}}$ coincide, and all other ODMNS are biaxial. Degree of biaxiality can be quantified by the relative differences between the eigenvalues or with the help of the parameter w (Eq. **25**). In Fig. 6, we present $w(\overline{\boldsymbol{Q}})$ in black and $\overline{w}$ in red, and one sees that N_{TB} and $N_{\mathrm{TB}e}$ are weakly biaxial, as $|\overline{w}| < 1$, while N_{SB} is always biaxial, passing the point of maximal biaxiality. Finally, $N^*_{\mathrm{SB}p}$ is biaxial of the oblate type, and N_p is uniaxial oblate. A further important characteristic of ODMNS presented in Fig. 3 is the variation of the wave vector with the field, which is shown in Fig. 7. Clearly, the wave vector vanishes in homogeneous nematic phases. Note that the general effect of the field is to unwind the structures, except for the initial behavior of $N_{\mathrm{TB}e}$, which is just the opposite. Another variable that characterizes ODMNS is the conical angle. This tilt angle is measured between **k** and $\hat{\mathbf{n}}$ but could also be given, for example, between **k** and $\hat{\mathbf{m}}$. Being constant for N_{TB}, it varies with z for all remaining ODMNS, as shown in Fig. 8, where we depict its minimal and maximal value with the field. It is apparent that both semiaxes of ellipse are equal in N_{TB} (blue and orange lines in Fig. 8 coincide), but a higher field makes the diameter of the cone's basis smaller. In $N_{\mathrm{TB}e}$, blue and orange lines split, providing the elliptic profile of the cone's basis. In the N_{SB} phase, the minimal value of that angle is equal to zero, and $\hat{\mathbf{m}}$ (Fig. 9) is perpendicular to **k**, which means that $\hat{\mathbf{n}}$ performs in-plane modulations between minimal and maximal values of $\theta_{\hat{\mathbf{n}}}$. Then, comparing Fig. 8 with Fig. 9 for the angle between **k** and $\hat{\mathbf{m}}$ gives insight into changing the primary director from $\hat{\mathbf{n}}$ to $\hat{\mathbf{m}}$ as the field increases for materials with negative anisotropy. This effect occurs when $\Delta\epsilon E^2 \cong -0.8$, and it is in fact caused by passing through a point of maximal biaxiality from prolate- to oblate-like structure, as shown in Fig. 6 for $\overline{w}$. Finally, in Fig. 10, we present the averages over one period for the length of polarization vector. The average of polarization modulus shows the average length of **P** for each structure, whereas the modulus of averaged polarization reveals which of the phases possess the uniform component of polarization.

Discussion

Scientists have long sought to understand how chiral states can be generated in a liquid state from nonchiral matter. Now strong evidence is found that a new class of nematics, called nematic twist–bend, provides such an example. This entropically induced state is realized because the underlying molecules have a specific

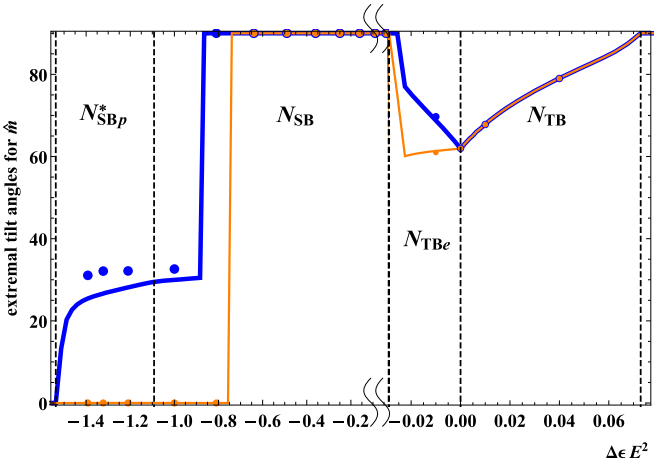

Fig. 9. Minimal (orange) and maximal (blue) values of angle between **k** and $\hat{\mathbf{m}}$. As previously, points are from the relaxation method, and lines are outcomes of the free-energy minimization with respect to the Fourier amplitudes for $n_{max} = 2$.

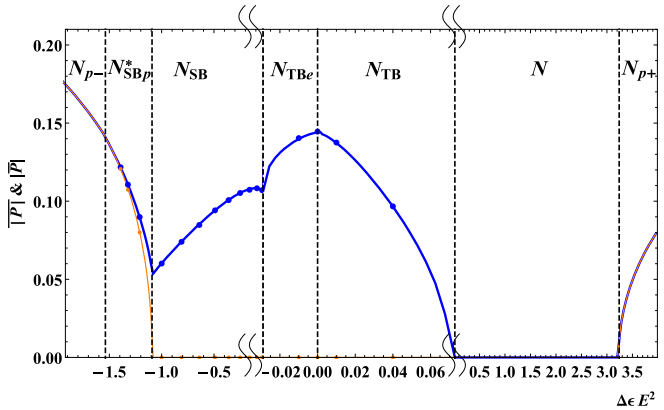

Fig. 10. Averages over one period of $|\overline{\boldsymbol{P}}|$ (blue) and $|\bar{\boldsymbol{P}}|$ (orange). As previously, points are from the relaxation method, and lines are outcomes of the free-energy minimization with respect to the Fourier amplitudes for $n_{max} = 2$.

shape. Here we presented possible transformations of the N_{TB} phase with an external field within the LdeG theory of flexopolarization. The outcomes of numerical minimization along with the full free-energy relaxation method have been studied for few sets of model parameters, with one typical example being discussed in-depth here.

For materials with positive anisotropy, the unwinding of the helix to the uniaxial (prolate) nematic structure is obtained, however here for sufficiently strong fields, a polar nematic appears more stable. Interestingly, in the N_{TB} phase, the circular cone of the director (Fig. 1) stays circular, while both periodicity of the structure and $\theta_{\hat{\mathbf{n}}}$ decrease with field. We do not observe an intermediate N_{SB} ordering, although such possibility cannot be excluded, in general. N_{SB} phase was expected as an intermediate state between neighboring N_{TB} domains with opposite chiralities (19). Compounds with negative material anisotropy give rise to three different ODMNS with a wide range of the N_{SB} phase, so it is an apparent suggestion that this phase can indeed be stabilized when applying external fields. Here N_{SB} appears almost universally through the mechanism of flattening the circular cone, where N_{TB} is converted into $N_{\mathrm{TB}e}$, even for infinitesimally small fields. Finally, we would like to add that in some cases studied the predicted $N^*_{\mathrm{SB}p}$ phase was replaced by an oblate nematic phase.

An interesting question that is left is whether currently available applied fields allow for potential experimental verification of our predictions. A connection between the physical and reduced fields can be estimated by a direct replacement of the LdeG parameters with their director field equivalents, akin to ref. 67. Since $\tilde{\mathbf{E}}$ couples to $\tilde{\mathbf{Q}}$, a natural estimate is that the field contribution $(-\varepsilon_0 \Delta\varepsilon \tilde{E}^2)$ should be of the same order of magnitude as the Frank elastic free energy stored in N_{TB}. This gives

$$\tilde{E}^2 \approx \frac{\pi^2}{p^2 |\Delta\varepsilon| \varepsilon_0} [K_{22} + K_{33} + (K_{33} - K_{22}) \cos(2\,\theta_{\hat{\mathbf{n}}})] \sin^2(\theta_{\hat{\mathbf{n}}}), \qquad [30]$$

where K_{22} (twist) and K_{33} (bend) are Frank elastic constants in the nematic phase, and $p = 2\pi/k$ is the pitch and k is the wave vector of N_{TB}. We do not know the elastic constants of the family of unwound nematic states stabilized at reference point A of Fig. 2, but owing that A should be only up to a few degrees of Kelvin away from the isotropic and the nematic phases ($t_Q > 0$), we assume that for compounds exhibiting the N_{TB} phase within the temperature range of 0 K to 10 K from the isotropic phase, the elastic constants are similar to those of CB7CB from ref. 67 within the same temperature range and that instability to N_{TB} requires very small values of K_{33}—that is, $K_{22} \lesssim 3$ pN and $K_{33} \lesssim 0.5$ pN. Taking in addition $\Delta\epsilon \approx 3$, $\theta_{\hat{\mathbf{n}}} \approx 20^\circ$, and $p \approx 10$ nm, it gives $\tilde{E} \sim 26$ V/μm. Please note that if the period of N_{TB} is in a range of 10 nm to 50 nm (68), the expected field strength can be reduced to 5 V/μm. Similar crude estimates for a mesogen with negative anisotropy and stable N_{TB}, where DTC5C9 (69) can serve as an example, gives the field range between 11 V/μm and 54 V/μm. Parameters used for these estimates are $\Delta\varepsilon \approx -0.6$, $K_{22} \approx 2$ pN, and $K_{33} \approx 0.5$ pN. The period's range of N_{TB} and the conical angle are taken as previously. As we can see, for an experimental test of the theory, it would be helpful to use a material with high dielectric anisotropy and large pitch. We should mention that typical fields currently used to study N_{TB} are of the order of 10 V/μm (20, 70). The contribution to the free energy due to a magnetic field has the same mathematical form as that of the electric field. Replacing $\tilde{E}$ with $\tilde{B}$ and $\frac{1}{|\Delta\varepsilon|\varepsilon_0}$ with $\frac{\mu_0}{|\Delta\chi|}$ in Eq. **30** and taking $\Delta\chi \approx 1.5 \times 10^{-6}$ SI units from ref. 67, we find that the magnetic field of the order of 10 T has the same effect as an electric field of about 1 V/μm.

If the nematic twist–bend phase is separated from the isotropic phase by the uniaxial nematic, we can set the scale for the field from properties of this intermediate nematic phase (Eq. **4**). A connection between the physical and reduced fields requires in this case an estimate of b and c parameters (Eq. **13**). One may also find it useful to know a_{0Q} and the elastic constant L_1 to set the temperature scale and correlate the experimental wave vector $\tilde{\mathbf{k}}$ of N_{TB} with $\mathbf{k}$ (Eq. **13**). More specifically, for $\tilde{\mathbf{E}} = \tilde{\mathbf{P}} = 0$ and under the assumption that $\tilde{\mathbf{Q}}$ is uniaxial,

$$\tilde{Q}_{\alpha\beta}(\tilde{\mathbf{r}}) = S\left(n_\alpha(\tilde{\mathbf{r}}) n_\beta(\tilde{\mathbf{r}}) - \frac{\delta_{\alpha\beta}}{3}\right), \qquad [31]$$

the free-energy density $\tilde{f}$ becomes reduced to that of the nematic phase expressed in terms of the scalar order parameter S and supplemented by splay, bend, and twist elastic deformation terms of the director ($\tilde{f} \to \tilde{f}(S, \hat{\mathbf{n}})$; see refs. 38 and 39). Please bear in mind that in agreement with the convention given by Eq. **2**, $S = 1$ for perfect orientational order and $S = 0$ for complete orientational disorder, which implies that

$$S\Delta\varepsilon_{max} = \Delta\varepsilon. \qquad [32]$$

A comparison of $\tilde{f}(S, \hat{\mathbf{n}})$ with Frank free-energy density and minimization with respect to S allows us to express a_{0Q}, b, c, L_1, and L_2 through various quantities that characterize nematic phase like the nematic–isotropic transition temperature T_{NI}, jump S_{NI} of the scalar order parameter at T_{NI}, transition entropy $\Delta\Sigma_{\mathrm{NI}}$, susceptibility anisotropy $\Delta\varepsilon_{\mathrm{NI}}$, spinodal temperature T^*, and Frank elastic constants K_{11} (splay), K_{22} (twist), and K_{33} (bend). The explicit formulas are (38)

$$a_{0Q} = \frac{3\,\Delta\Sigma_{\mathrm{NI}}}{2\,S_{\mathrm{NI}}^2}, \qquad b = \frac{9\,\Delta\Sigma_{\mathrm{NI}}\,(T_{\mathrm{NI}} - T^*)}{S_{\mathrm{NI}}^3}, \qquad [33]$$

$$c = \frac{9\,\Delta\Sigma_{\mathrm{NI}}\,(T_{\mathrm{NI}} - T^*)}{4 S_{\mathrm{NI}}^4}. \qquad [34]$$

The relations for L_1 and L_2 read (39)

$$L_1 \approx \frac{K_{22,2}}{4}, \qquad L_2 \approx \frac{K_{11,2} - 2K_{22,2} + K_{33,2}}{4}. \qquad [35]$$

They are accurate up to S^2 for K_{ii} expanded in terms of S ($K_{ii} \approx K_{ii,2}S^2 + K_{ii,3}S^3 + \cdots$) and should be treated with caution. The reason is that the experimental data show huge anisotropy

of splay–bend elastic constants. While K_{11} and K_{22} generally increase with decreasing temperature following the S^2 dependence predicted by the minimal coupling LdeG model, the nonmonotonic temperature variation of K_{33} cannot be explained. A quantitative theory of $N_{\rm TB}$ would then require the presence of higher order elastic invariants of the form $\mathbf{Q}(\nabla\mathbf{Q})^2$, three of which are relevant, and the stabilizing terms $(\mathbf{Q}\nabla\mathbf{Q})^2$ (39). Assuming qualitative agreement and applying formulas Eqs. **33**–**35**, in Eq. **13** one can obtain a different relation between the dimensionless and physical fields, expressed in terms of experimentally accessible quantities at the nematic–isotropic phase transition. More precisely,

$$\tilde{E}^2 = \frac{288\,\Delta\Sigma_{\rm NI}\,(T_{\rm NI}-T^*)}{\varepsilon_0\,\Delta\varepsilon_{\rm NI}}\,\Delta\epsilon\,E^2, \qquad \textbf{[36]}$$

where T^* can be found, for example, by fitting theoretically predicted temperature variation of S

$$S = \frac{3}{4}S_{\rm NI}\left\{1+\left[1-\frac{8(T-T^*)}{9(T_{\rm NI}-T^*)}\right]^{\frac{1}{2}}\right\} \qquad \textbf{[37]}$$

to experimental data. Using exemplary data for CB7CB from refs. 3 and 67, $\Delta\Sigma_{\rm NI}\approx 0.34R$, $\Delta\varepsilon_{\rm NI}\approx 1.5$, and $T_{NI}-T^*\approx 89$ mK [our fit to experimental data for S (67) using Eq. **37** gives a somewhat higher value of 0.1 K]; mass density $\rho\approx 10^3$ kg/m^3; and molar mass $M\approx 0.45$ kg/mol, we get $\tilde{E}\approx 110\,[V/\mu m]\sqrt{|\Delta\epsilon\,E^2|}$, which yields $\tilde{E}\approx 27[V/\mu m]$. Note that the two independently determined estimates of the field agree surprisingly well.

The final remark is that fields analyzed in this paper can also be of surface Rapini–Papoular form (11): $\tilde{f}_E = r_p \mathrm{Tr}\,[\mathbf{Q}(z)-\mathbf{Q}(z_0)]^2\delta(z-z_0)$, with $z_0=0, L$, for their relevant part, which is uniaxial given by Eq. **31**, has a similar mathematical structure as Eq. **18**, where the role of external field $\hat{e}_\gamma$ is taken by the surface preferred orientation $n_\gamma(0)\equiv n_\gamma(\tilde{z}_0)$. Indeed, this contribution is proportional to $n_\alpha(0)\tilde{Q}_{\alpha\beta}(\mathbf{r})n_\beta(0)$, and for planar anchoring, we may expect a surface-induced $N_{\rm TBe}$ ordering, irrespective of the strength of r_p. Clearly, this remark refers only to a very narrow region close to the surfaces. Observations of chiral phase with the presence of splay and bend deformations (2, 70, 71) obtained under both surface and alternating electric fields or evidence of the second $N_{\rm TB}$ phase (20) may indicate that some phase transformations under external fields we predicted have already been observed. However, here we did not consider the presence of two (perpendicular) fields instantly, which may lead to stabilization of new structures besides the ODMNS class, with simultaneous modulation in more than one direction.

Closing Note. While our paper was subject to the reviewing procedure, we have learned that Merkel et al. (72) have confirmed experimentally the electric field-stabilized N_{TBe} and N_{SB} phases for a bent-core liquid crystal compound with negative dielectric anisotropy. They applied direct electric fields of the order of 5 V/μm.

ACKNOWLEDGMENTS. We thank the referees and the editor for valuable comments. This work was supported by National Science Center in Poland Grant DEC-2013/11/B/ST3/04247. G.P. acknowledges the support of Cracowian Consortium "Materia-Energia-Przyszłość im. Mariana Smoluchowskiego" within the "Krajowy Naukowy Ośrodek Wiodący" (KNOW) grant.

1. Šepelj M, et al. (2007) Intercalated liquid-crystalline phases formed by symmetric dimers with an α,ω-diiminoalkylene spacer. *J Mater Chem* 17:1154–1165.
2. Panov VP, et al. (2010) Spontaneous periodic deformations in nonchiral planar-aligned bimesogens with a nematic-nematic transition and a negative elastic constant. *Phys Rev Lett* 105:167801.
3. Cestari M, et al. (2011) Phase behavior and properties of the liquid-crystal dimer 1",7"-bis(4-cyanobiphenyl-4'-yl) heptane: A twist-bend nematic liquid crystal. *Phys Rev E* 84:031704.
4. Borshch V, et al. (2013) Nematic twist-bend phase with nanoscale modulation of molecular orientation. *Nat Commun* 4:2635.
5. Chen D, et al. (2013) Chiral heliconical ground state of nanoscale pitch in a nematic liquid crystal of achiral molecular dimers. *Proc Natl Acad Sci USA* 110:15931–15936.
6. Paterson DA, et al. (2016) Understanding the twist-bend nematic phase: The characterisation of 1-(4-cyanobiphenyl-4'-yloxy)-6-(4-cyanobiphenyl-4'-yl)hexane (cb6ocb) and comparison with cb7cb. *Soft Matter* 12:6827–6840.
7. López DO, et al. (2016) Miscibility studies of two twist-bend nematic liquid crystal dimers with different average molecular curvatures. A comparison between experimental data and predictions of a Landau mean-field theory for the NTB-N phase transition. *Phys Chem Chem Phys* 18:4394–4404.
8. Görtz V, Southern C, Roberts NW, Gleeson HF, Goodby JW (2009) Unusual properties of a bent-core liquid-crystalline fluid. *Soft Matter* 5:463–471.
9. Chen D, et al. (2014) Twist-bend heliconical chiral nematic liquid crystal phase of an achiral rigid bent-core mesogen. *Phys Rev E* 89:022506.
10. Wang Y, et al. (2015) Room temperature heliconical twist-bend nematic liquid crystal. *CrystEngComm* 17:2778–2782.
11. de Gennes PG, Prost J (1993) *The Physics of Liquid Crystals* (Oxford Univ Press, New York), 2 Ed.
12. Dozov I (2001) On the spontaneous symmetry breaking in the mesophases of achiral banana-shaped molecules. *Europhys Lett* 56:247–253.
13. Meyer RB (1969) Piezoelectric effects in liquid crystals. *Phys Rev Lett* 22:918–921.
14. Meyer RB (1976) Structural problems in liquid crystal physics. *Proceedings of the Les Houches Summer School on Theoretical Physics, 1973, Session No. XXV*, eds Balian R, Weil G (Gordon and Breach, New York), pp 271–343.
15. Karbowniczek P, Cieśla M, Longa L, Chrzanowska A (2017) Structure formation in monolayers composed of hard bent-core molecules. *Liq Cryst* 44:254–272.
16. Adlem K, et al. (2013) Chemically induced twist-bend nematic liquid crystals, liquid crystal dimers, and negative elastic constants. *Phys Rev E* 88:022503.
17. Longa L, Trebin HR (1990) Spontaneous polarization in chiral biaxial liquid crystals. *Phys Rev A* 42:3453–3469.
18. Longa L, Pająk G (2016) Modulated nematic structures induced by chirality and steric polarization. *Phys Rev E* 93:040701.
19. Meyer C, Luckhurst GR, Dozov I (2015) The temperature dependence of the heliconical tilt angle in the twist-bend nematic phase of the odd dimer cb7cb. *J Mater Chem C* 3:318–328.
20. Sreenilayam SP, Panov VP, Vij JK, Shanker G (2017) The NTB phase in an achiral asymmetrical bent-core liquid crystal terminated with symmetric alkyl chains. *Liq Cryst* 44:244–253.
21. Zhu C, et al. (2016) Resonant carbon *k*-edge soft x-ray scattering from lattice-free heliconical molecular ordering: Soft dilative elasticity of the twist-bend liquid crystal phase. *Phys Rev Lett* 116:147803.
22. Stevenson WD, et al. (2017) Molecular organization in the twist-bend nematic phase by resonant x-ray scattering at the se k-edge and by SAXS, WAXS and GIXRD. *Phys Chem Chem Phys* 19:13449–13454.
23. Archbold CT, Davis EJ, Mandle RJ, Cowling SJ, Goodby JW (2015) Chiral dopants and the twist-bend nematic phase–induction of novel mesomorphic behaviour in an apolar bimesogen. *Soft Matter* 11:7547–7557.
24. Dawood AA, et al. (2016) On the twist-bend nematic phase formed directly from the isotropic phase. *Liq Cryst* 43:2–12.
25. Memmer R (2002) Liquid crystal phases of achiral banana-shaped molecules: A computer simulation study. *Liq Cryst* 29:483–496.
26. Shamid SM, Dhakal S, Selinger JV (2013) Statistical mechanics of bend flexoelectricity and the twist-bend phase in bent-core liquid crystals. *Phys Rev E* 87:052503.
27. Greco C, Luckhurst GR, Ferrarini A (2014) Molecular geometry, twist-bend nematic phase and unconventional elasticity: A generalised Maier-Saupe theory. *Soft Matter* 10:9318–9323.
28. Greco C, Ferrarini A (2015) Entropy-driven chiral order in a system of achiral bent particles. *Phys Rev Lett* 115:147801.
29. Osipov MA, Pająk G (2016) Effect of polar intermolecular interactions on the elastic constants of bent-core nematics and the origin of the twist-bend phase. *Eur Phys J E* 39:45.
30. Vanakaras AG, Photinos DJ (2016) A molecular theory of nematic-nematic phase transitions in mesogenic dimers. *Soft Matter* 12:2208–2220.
31. Ferrarini A (2017) The twist-bend nematic phase: Molecular insights from a generalised Maier–Saupe theory. *Liq Cryst* 44:45–57.
32. Osipov MA, Pająk G (2017) Polar interactions between bent–core molecules as a stabilising factor for inhomogeneous nematic phases with spontaneous bend deformations. *Liq Cryst* 44:58–67.
33. Tomczyk W, Pająk G, Longa L (2016) Twist-bend nematic phases of bent-shaped biaxial molecules. *Soft Matter* 12:7445–7452.
34. Mandle RJ, et al. (2014) Synthesis and characterisation of an unsymmetrical, ether-linked, fluorinated bimesogen exhibiting a new polymorphism containing the n(tb) or 'twist-bend' phase. *Phys Chem Chem Phys* 16:6907–6915.
35. Ivsic T, Vinkovic M, Baumeister U, Mikleusevic A, Lesac A (2014) Retracted article: Milestone in the NTB phase investigation and beyond: Direct insight into molecular self-assembly. *Soft Matter* 10:9334–9342.
36. Mandle RJ, et al. (2015) Apolar bimesogens and the incidence of the twist-bend nematic phase. *Chem A Eur J* 21:8158–8167.

37. Longa L, Pająk G (2016) *Phys Rev E* 93:040701(R). Modulated nematic structures induced by chirality and steric polarization. Available at journals.aps.org/pre/supplemental/10.1103/PhysRevE.93.040701/Supplemental_material.pdf. Accessed April 18, 2016.
38. Gramsbergen EF, Longa L, de Jeu WH (1986) Landau theory of the nematic-isotropic phase transition. *Phys Rep* 135:195–257.
39. Longa L, Monselesan D, Trebin HR (1987) An extension of the Landau-Ginzburg-de Gennes theory for liquid crystals. *Liq Cryst* 2:769–796.
40. Parsouzi Z, et al. (2016) Fluctuation modes of a twist-bend nematic liquid crystal. *Phys Rev X* 6:021041.
41. Lubensky TC, Radzihovsky L (2002) Theory of bent-core liquid-crystal phases and phase transitions. *Phys Rev E* 66:031704.
42. Brand HR, Pleiner H, Cladis PE (2005) Tetrahedratic cross-couplings: Novel physics for banana liquid crystals. *Physica A* 351:189–197.
43. Longa L, Pająk G, Wydro T (2009) Chiral symmetry breaking in bent-core liquid crystals. *Phys Rev E* 79:040701.
44. Longa L, Pająk G (2011) Generalized dispersion model of orientationally ordered phases of bent–core liquid crystals. *Mol Cryst Liq Cryst* 541:152/[390]–158/[396].
45. Trojanowski K, Pająk G, Longa L, Wydro T (2012) Tetrahedratic mesophases, chiral order, and helical domains induced by quadrupolar and octupolar interactions. *Phys Rev E* 86:011704.
46. Longa L, Trojanowski K (2013) Ambidextrous chiral domains in nonchiral liquid-crystalline materials. *Acta Phys Pol B* 44:1201.
47. Trojanowski K, Cieśla M, Longa L (2017) Modulated nematic structures and chiral symmetry breaking in 2D. *Liq Cryst* 44:273–283.
48. Srigengan S, et al. (2018) Anomalously low twist and bend elastic constants in an oxadiazole-based bent-core nematic liquid crystal and its mixtures; contributions of spontaneous chirality and polarity. *J Mater Chem C* 6:980–988.
49. Deuling HJ (1972) Deformation of nematic liquid crystals in an electric field. *Mol Cryst Liq Cryst* 19:123–131.
50. Xiang J, et al. (2015) Electrically tunable selective reflection of light from ultraviolet to visible and infrared by heliconical cholesterics. *Adv Mater* 27:3014–3018.
51. Salili SM, et al. (2016) Magnetically tunable selective reflection of light by heliconical cholesterics. *Phys Rev E* 94:042705.
52. Meyer RB (1968) Effects of electric and magnetic fields on the structure of cholesteric liquid crystals. *Appl Phys Lett* 12:281–282.
53. Scarfone AM, Lelidis I, Barbero G (2011) Cholesteric-nematic transition induced by a magnetic field in the strong-anchoring model. *Phys Rev E* 84:021708.
54. Zakhlevnykh AN, Shavkunov VS (2016) Magnetic-field-induced stepwise director reorientation and untwisting of a planar cholesteric structure with finite anchoring energy. *Phys Rev E* 94:042708.
55. Yang DK, Wu ST (2001) *Reflective Liquid Crystal Displays, Wiley SID Series in Display Technology* (Wiley, Chichester, UK).
56. Challa PK, et al. (2014) Twist-bend nematic liquid crystals in high magnetic fields. *Phys Rev E* 89:060501.
57. Salili SM, et al. (2016) Anomalous increase in nematic-isotropic transition temperature in dimer molecules induced by a magnetic field. *Phys Rev Lett* 116:217801.
58. Meyer C (2016) Nematic twist-bend phase under external constraints. *Liq Cryst* 43:2144–2162.
59. Zola RS, Barbero G, Lelidis I, Rosseto MP, Evangelista LR (2017) A continuum description for cholesteric and nematic twist-bend phases based on symmetry considerations. *Liq Cryst* 44:24–30.
60. Shiyanovskii SV, Simonário PS, Virga EG (2017). Coarse-graining elastic theory for twist-bend nematic phases. *Liq Cryst* 44:31–44.
61. Longa L (1986) On the tricritical point of the nematic–smectic a phase transition in liquid crystals. *J Chem Phys* 85:2974.
62. Longa L, Grzybowski P, Romano S, Virga E (2005) Minimal coupling model of the biaxial nematic phase. *Phys Rev E* 71:051714.
63. Allender D, Longa L (2008) Landau-de Gennes theory of biaxial nematics reexamined. *Phys Rev E* 78:011704.
64. Alexander GP, Yeomans JM (2006) Stabilizing the blue phases. *Phys Rev E* 74:061706.
65. Henrich O, Marenduzzo D, Stratford K, Cates ME (2010) Thermodynamics of blue phases in electric fields. *Phys Rev E* 81:031706.
66. Alexander GP, Yeomans JM (2007) Flexoelectric blue phases. *Phys Rev Lett* 99:067801.
67. Babakhanova G, et al. (2017) Elastic and viscous properties of the nematic dimer cb7cb. *Phys Rev E* 96:062704.
68. Ewa G, et al. (2015) A twist-bend nematic (NTB) phase of chiral materials. *Angew Chem Int Ed* 54:10155–10159.
69. Cukrov G, et al. (2017) Comparative analysis of anisotropic material properties of uniaxial nematics formed by flexible dimers and rod-like monomers. *Liquid Crystals* 44:219–231.
70. Panov VP, et al. (2012) Field-induced periodic chiral pattern in the NX phase of achiral bimesogens. *Appl Phys Lett* 101:234106.
71. Panov VP, et al. (2011) Microsecond linear optical response in the unusual nematic phase of achiral bimesogens. *Appl Phys Lett* 99:261903.
72. Merkel K, Kocot A, Vij JK, Shanker G (2018) Distortions in structures of the twist bend nematic phase of a bent-core liquid crystal by the electric field. *Phys Rev E* 98:022704.